



HAL
open science

The Mycobacterium tuberculosis Ser/Thr kinase substrate Rv2175c is a DNA-binding protein regulated by phosphorylation.

Martin Cohen-Gonsaud, Philippe Barthe, Marc J Canova, Charlotte Stagier-Simon, Laurent Kremer, Christian Roumestand, Virginie Molle

► To cite this version:

Martin Cohen-Gonsaud, Philippe Barthe, Marc J Canova, Charlotte Stagier-Simon, Laurent Kremer, et al.. The Mycobacterium tuberculosis Ser/Thr kinase substrate Rv2175c is a DNA-binding protein regulated by phosphorylation.. Journal of Biological Chemistry, 2009, 284 (29), pp.19290-19300. 10.1074/jbc.M109.019653 . hal-00458843

HAL Id: hal-00458843

<https://hal.science/hal-00458843>

Submitted on 27 May 2021

HAL is a multi-disciplinary open access archive for the deposit and dissemination of scientific research documents, whether they are published or not. The documents may come from teaching and research institutions in France or abroad, or from public or private research centers.

L'archive ouverte pluridisciplinaire **HAL**, est destinée au dépôt et à la diffusion de documents scientifiques de niveau recherche, publiés ou non, émanant des établissements d'enseignement et de recherche français ou étrangers, des laboratoires publics ou privés.



Distributed under a Creative Commons Attribution 4.0 International License

The *Mycobacterium tuberculosis* Ser/Thr Kinase Substrate Rv2175c Is a DNA-binding Protein Regulated by Phosphorylation*

Received for publication, March 16, 2009, and in revised form, May 11, 2009. Published, JBC Papers in Press, May 20, 2009, DOI 10.1074/jbc.M109.019653

Martin Cohen-Gonsaud^{†‡§¶1}, Philippe Barthe^{†§¶1}, Marc J. Canova^{||}, Charlotte Stagier-Simon^{†§¶1}, Laurent Kremer^{**‡‡‡}, Christian Roumestand^{†‡§¶1}, and Virginie Molle^{||2}

From [†]CNRS UMR 5048, Centre de Biochimie Structurale, Montpellier, [§]INSERM U554, Montpellier, and the [¶]Université Montpellier I et II, 34090 Montpellier, the ^{||}Institut de Biologie et Chimie des Protéines, CNRS UMR 5086, Université Lyon 1, IFR128 BioSciences, Lyon-Gerland, 69367 Lyon, the ^{**}Laboratoire de Dynamique des Interactions Membranaires Normales et Pathologiques (DIMNP), Universités de Montpellier II et I, CNRS UMR 5235, case 107, Place Eugène Bataillon, 34095 Montpellier Cedex 05, and ^{‡‡}INSERM, DIMNP, Place Eugène Bataillon, 34095 Montpellier Cedex 05, France

Recent efforts have underlined the role of serine/threonine protein kinases in growth, pathogenesis, and cell wall metabolism in *Mycobacterium tuberculosis*. Although most kinases have been investigated for their physiological roles, little information is available regarding how serine/threonine protein kinase-dependent phosphorylation regulates the activity of kinase substrates. Herein, we focused on *M. tuberculosis* Rv2175c, a protein of unknown function, conserved in actinomycetes, and recently identified as a substrate of the PknL kinase. We solved the solution structure of Rv2175c by multidimensional NMR and demonstrated that it possesses an original winged helix-turn-helix motif, indicative of a DNA-binding protein. The DNA-binding activity of Rv2175c was subsequently confirmed by fluorescence anisotropy, as well as in electrophoretic mobility shift assays. Mass spectrometry analyses using a combination of MALDI-TOF and LC-ESI/MS/MS identified Thr⁹ as the unique phosphoacceptor. This was further supported by complete loss of PknL-dependent phosphorylation of an Rv2175c_T9A mutant. Importantly, the DNA-binding activity was completely abrogated in a Rv2175c_T9D mutant, designed to mimic constitutive phosphorylation, but not in a mutant lacking the first 13 residues. This implies that the function of the N-terminal extension is to provide a phosphoacceptor (Thr⁹), which, following phosphorylation, negatively regulates the Rv2175c DNA-binding activity. Interestingly, the N-terminal disordered extension, which bears the phosphoacceptor, was found to be restricted to members of the *M. tuberculosis* complex, thus suggesting

the existence of an original mechanism that appears to be unique to the *M. tuberculosis* complex.

In response to its environment, *Mycobacterium tuberculosis* (*M. tb*)³ activates or represses the expression of a number of genes to promptly adjust to new conditions. More precisely, during the infection process, cross-talk of signals between the host and the bacterium take place, resulting in reprogramming the host signaling network. Many of these stimuli are transduced in the bacteria via sensor kinases, enabling the pathogen to adapt its cellular response to survive in hostile environments. Although the two-component systems represent the classic prokaryotic mechanism for detection and response to environmental changes, the serine/threonine and tyrosine protein kinases (STPKs) associated with their phosphatases have emerged as important regulatory systems in prokaryotic cells (1–3). *M. tb* contains eleven STPKs (4, 5), and most are being investigated for their physiological roles and potential application for future drug development to combat tuberculosis (6). Through phosphorylation these STPKs are also thought to play important functions in cell signaling responses as well as in essential metabolic pathways. The cell wall of *M. tb* plays a critical role in the defense of this pathogen in the host, and changes in cell wall composition in response to various environmental stimuli are critical to *M. tb* adaptation during infection. Although little is known regarding the cell wall regulatory mechanisms in *M. tb*, there is now an increasing body of evidence indicating that these processes largely rely on STPK-dependent mechanisms (7–9).

Moreover, little information on the range of functions regulated by the STPKs is available, and the complicated mycobacterial phosphoproteome is still far from being deciphered. Understanding mycobacterial kinase biology has been severely impeded by the difficulty to identify direct kinase substrates and the subsequent characterization of the phosphorylation site(s). However, several recent studies have reported the iden-

* This work was supported by Agence Nationale de la Recherche Grants JC07_203251 (to M. C.-G.) and ANR-06-MIME-027-01 (to V. M. and L. K.). NMR experiments were recorded and analyzed using the facilities of the Structural Biology platform RIO (CBS, Montpellier, France).

The atomic coordinates and structure factors (code 2KFS) have been deposited in the Protein Data Bank, Research Collaboratory for Structural Bioinformatics, Rutgers University, New Brunswick, NJ (<http://www.rcsb.org/>).

The chemical shifts have been deposited in the BioMagResBank under the accession number BMRB-16188.

¹ To whom correspondence may be addressed: CNRS UMR 5048, Centre de Biochimie Structurale, 34090 Montpellier, France. Tel.: 33-4-67-41-79-06; Fax: 33-4-67-41-79-13; E-mail: martin@cbs.cnrs.fr.

² To whom correspondence may be addressed: Institut de Biologie et Chimie des Protéines, CNRS UMR 5086, Université Lyon 1, IFR128 BioSciences, Lyon-Gerland, 69367 Lyon, France. Tel.: 33-4-72-72-26-79; Fax: 33-4-72-72-26-41; E-mail: vmolle@ibcp.fr.

³ The abbreviations used are: *M. tb*, *M. tuberculosis*; EMSA, electrophoretic mobility shift assay; STPK, Ser/Thr protein kinase; TEV, tobacco etch virus; HSQC, heteronuclear single quantum coherence; HTH, helix-turn-helix; wHTH, winged HTH; MS, mass spectrometry.

tification and characterization of the phosphorylation sites in substrates related to various metabolic pathways in mycobacteria. These include the Fork Head associated-containing protein GarA, a key regulator of the tricarboxylic cycle (10, 11); PbpA, a penicillin-binding protein required for cell division (12); Wag31, a homologue of the cell division protein DivIVA that regulates growth, morphology, and polar cell wall biosynthesis in mycobacteria (13); the β -ketoacyl acyl carrier protein synthase mtFabH, which participates in mycolic acid biosynthesis (9); the anti-anti-sigma factor Rv0516c (14); the alternate sigma factor SigH, which is a central regulator of the response to oxidative stress (15); as well as the essential mycobacterial chaperone GroEL1 (16).

Therefore, a further characterization of STPKs substrates is critical to unraveling the mechanisms by which STPK-dependent phosphorylation induces modifications, thus regulating their activity, ultimately conditioning biological responses in mycobacteria. Such studies may also provide the key to designing new inhibitors that target signal transduction pathways specific to *M. tb*.

We recently characterized a novel substrate/kinase pair in *M. tb*, PknL/Rv2175c (17). *pknL* is associated with the ~30-kb *dcw* (division cell wall) gene cluster, which encompasses several genes involved in cell wall synthesis and cell division (17, 18), raising the possibility that PknL might participate in the regulation of this gene cluster. Moreover, *pknL* (Rv2176) is adjacent to the *Rv2175c* gene, encoding a 16-kDa protein of unknown function. We further demonstrated that phosphorylation of the activation loop Thr-173 residue was required for optimal PknL-mediated phosphorylation of Rv2175c. Moreover, Rv2175c belongs to a mycobacterial "core" of 219 genes, identified by macroarray and bioinformatic analysis, common to *M. tb*- and *Mycobacterium leprae*-encoding proteins showing no similarity with proteins from other organisms. The presence of Rv2175c as a member of this set of genes emphasizes the importance of Rv2175c in the physiology of *M. tb*. In this context, we reasoned that the structural determination of Rv2175c would provide a valuable basis for a better understanding of the function of this protein.

Therefore, we have undertaken the structural determination of Rv2175 using multidimensional NMR techniques. Herein, we provide strong evidence that Rv2175c is a DNA-binding protein and investigated how phosphorylation of a unique Thr residue in the N-terminal domain of the protein affects its DNA-binding activity.

EXPERIMENTAL PROCEDURES

Bacterial Strains and Growth Conditions—Strains used for cloning and expression of recombinant proteins were *Escherichia coli* DH5 α (Invitrogen) and *E. coli* BL21(DE3)Star (Novagen). Strains were grown at 37 °C in LB medium supplemented with 100 μ g/ml ampicillin.

Cloning, Expression, and Purification of Rv2175c and Mutant Proteins—The *Rv2175c* gene was amplified by PCR using *M. tuberculosis* H37Rv genomic DNA as a template and the following primers: #403, 5'-TAT ATA TCG TT CAT atg CCT GGC CGC GCA CCA GGC TCT-3' (containing an NdeI restriction site underlined) and, #404, 5'-TAT GGA TCC TCA ATA CGC

CAT AGC CTG GGC CCG-3' (containing a BamHI restriction site underlined). This 441-bp amplified product was digested by NdeI and BamHI and ligated into pET15bTev, the variant of pET15b (Novagen) that includes the replacement of the thrombin site coding sequence with a tobacco etch virus (TEV) protease site (19), and in pETPhos, the variant of pET15bTev that is devoid of putative phosphoacceptors in the His tag fusion (20), thus generating pET15bTev_Rv2175c and pETPhos_Rv2175c, respectively. Site-directed mutagenesis was directly performed on pETPhos_Rv2175c using inverse-PCR amplification with the following self-complementary primers: 5'-GGC CGC GCA CCA GGC TCT **GCA** CTT GCG CGG GTG GGC AGC-3' and 5'-GCT GCC CAC CCG CGC AAG TGC AGA GCC TGG TGC GCG GCC-3' for Rv2175_T9A, 5'-GGC CGC GCA CCA GGC TCT **GAC** CTT GCG CGG GTG GGC AGC-3' and 5'-GCT GCC CAC CCG CGC AAG **GTC** AGA GCC TGG TGC GCG GCC-3' for Rv2175_T9D, 5'-GGC CGC GCA CCA GGC TCT **GAA** CTT GCG CGG GTG GGC AGC-3' and 5'-GCT GCC CAC CCG CGC AAG **TTC** AGA GCC TGG TGC GCG GCC-3' for Rv2175_T9E (the corresponding substitutions are shown in bold). The Rv2175c N-terminal truncated fragment lacking the first 13 residues was amplified by PCR using *M. tuberculosis* H37Rv genomic DNA as a template and the following primers: #615, 5'-TAA TAG CTC ATA TGG GCA GCA TTC CCG CTG GCG ATG AC-3' (containing an NdeI restriction site underlined) and #404. This 402-bp amplified product was digested by NdeI and BamHI and ligated into pET15bTev thus generating pET15bTev_Rv2175c₁₄₋₁₄₆. All constructs were verified by DNA sequencing. Recombinant *E. coli* BL21(DE3)Star strains harboring the Rv2175c-expressing constructs pET15bTev_Rv2175c, pETPhos_Rv2175c, pETPhos_Rv2175c_T9A, pETPhos_Rv2175c_T9D, pETPhos_Rv2175c_T9E, and pET15bTev_Rv2175c₁₄₋₁₄₆ were used to inoculate 750 ml of LB medium supplemented with ampicillin and incubated at 37 °C with shaking. When A_{600} reached 0.6, isopropyl 1-thio- β -D-galactopyranoside was added at a final concentration of 0.2 mM, and growth was continued for an additional 3 h at 37 °C with shaking. Purifications of the His-tagged proteins were performed as reported previously (8, 21). When required, the protein was treated with TEV protease. Finally, the purified protein was concentrated and applied to a Superdex 75 26/60 (Amersham Biosciences) size exclusion column, equilibrated in buffer 20 mM sodium acetate, pH 4.6, 300 mM NaCl to remove any remaining impurities and the cleaved tag when TEV protease cleavage was performed. The purified Rv2175c protein were identified by SDS-PAGE and stored at -20 °C until required. This protocol was carried out for all the non-labeled constructs and ¹⁵N labeled of wild-type and mutant Rv2175c constructs, excepted that the cultures were grown in a minimum media containing ¹⁵NH₄Cl and ¹³C₆ glucose as the sole nitrogen and carbon sources.

Cloning, Expression, and Purification of the Recombinant PknL₁₋₂₈₁ Protein—The *pknL* PCR fragment encoding the kinase core domain corresponding to the kinase domain without the juxtamembrane linker of PknL (residues 1–281 out of 399) was amplified by PCR using *M. tuberculosis* H37Rv genomic DNA as a template and the following primers: #399, 5'-TAT CAT ATG CCG TTG GAG AGC GCG CTG CTG-3'

Solution Structure of *M. tuberculosis* Rv2175c

(containing an NdeI restriction site underlined) and, #400, 5'-TAT GGA TCC TTA CTC CTC GGC GAT CGC CTC CAG-3' (containing a BamHI restriction site underlined). This 843-bp amplified product was digested by NdeI and BamHI and ligated into pET15bTev. *E. coli* BL21(DE3)Star cells were transformed with the pET15bTev_pknL₁₋₂₈₁ vector expressing the PknL₁₋₂₈₁ core domain. Purifications of the His-tagged protein was performed as above (8, 21). When required, the protein was treated with TEV protease according to the manufacturer's instructions (Invitrogen).

Solution Structure of Rv2175c—NMR experiments were carried out at 14.1 Tesla on a Bruker Avance 600 spectrometer equipped with a 5-mm z-gradient ¹H-¹³C-¹⁵N triple resonance cryoprobe. ¹H, ¹³C, and ¹⁵N resonances were assigned using standard triple resonance three-dimensional experiments (22) recorded at 30 °C on 0.3 mM ¹⁵N- or ¹⁵N,¹³C-labeled Rv2175c protein samples dissolved in 10 mM sodium acetate, pH 4.6, 150 mM NaCl with 5% D₂O for the lock. ¹H chemical shifts were directly referenced to the methyl resonance of di-ethylsilapentane sulfonate, whereas ¹³C and ¹⁵N chemical shifts were referenced indirectly to the absolute frequency ratios ¹⁵N/¹H = 0.101329118 and ¹³C/¹H = 0.251449530. All NMR spectra were processed with GIFA (23). Nuclear Overhauser effect peaks identified on three-dimensional [¹H,¹⁵N] and [¹H,¹³C] three-dimensional nuclear Overhauser effect spectroscopy-HSQC were assigned through automated NMR structure calculations with CYANA 2.1 (24). Backbone ϕ and ψ torsion angle constraints were obtained from a data base search procedure on the basis of backbone (¹⁵N, HN, ¹³C', ¹³C α , H α , and ¹³C β) chemical shifts using the program TALOS (25). Hydrogen bond restraints were derived using standard criteria on the basis of the amide ¹H/²H exchange experiments and nuclear Overhauser effect data. When identified, the hydrogen bond was enforced using the following restraints: ranges of 1.8–2.3 Å for $d(\text{N-H},\text{O})$, and 2.7–3.3 Å for $d(\text{N},\text{O})$. The final list of restraints (from which values redundant with the covalent geometry have been eliminated) consisted of 477 intra-residues, 576 sequential, 278 medium-range ($1 < i-j \leq 4$), and 345 long range upper bound distance restraints, 190 backbone dihedral angle restraints (ϕ and ψ), and 66 hydrogen bond restraints. The 30 best structures (based on the final target penalty function values) were minimized with CNS 1.2 according to the RECOORD procedure (26) and analyzed with PROCHECK (27). The root mean square deviations were calculated with MOLMOL (28). Structural statistics are given in (Table 1).

Electrophoretic Mobility Shift Assays—The DNA fragment used in this assay corresponds to 200 bp of non-relevant double stranded *M. tuberculosis* DNA. The 5' ends of DNA were labeled using [γ -³²P]ATP and T4 polynucleotide kinase. A typical assay mixture contained in 20 μ l: 10 mM Tris-HCl, pH 7.5, 50 mM NaCl, 1 mM EDTA, 1 mM dithiothreitol, 5% (v/v) glycerol, 0.5 mg of bovine serum albumin, radioactive DNA probe (2000 cpm.ml⁻¹), and various amounts of the purified Rv2175c proteins. After 30 min of incubation at room temperature, 20 μ l of this mixture was loaded onto a native 4% (w/v) polyacrylamide TBE Ready Gel (Bio-Rad) and electrophoresed in 1% TBE (Tris-Borate-EDTA) buffer for 1 h at 100 V.cm⁻¹. Radioactive

TABLE 1
NMR and refinement statistics for Rv2175c protein structures

	Protein
NMR distance and dihedral constraints	
Distance constraints	
Total NOE	1676
Intra-residue	477
Inter-residue	
Sequential ($ i - j = 1$)	576
Medium range ($ i - j < 4$)	278
Long-range ($ i - j > 5$)	345
Intermolecular	
Hydrogen bonds	66
Total dihedral angle restraints	
ϕ	95
ψ	95
χ_1	17
Structure statistics	
Violations (mean \pm S.D.)	
Maximum distance constraint violation (Å)	0.16 \pm 0.02
Maximum dihedral angle violation (°)	4.00 \pm 0.88
Deviations from idealized geometry	
Bond lengths (Å)	0.0095 \pm 0.0002
Bond angles (°)	1.1437 \pm 0.0241
Improper (°)	1.2872 \pm 0.0643
Ramachandran plot (%)	
Most favored region	93.2
Additionally allowed region	6.4
Generously allowed region	0.3
Disallowed region	0.1
Average pairwise root mean square deviation^a (Å)	
Backbone	0.87 \pm 0.15
Heavy	1.54 \pm 0.18

^a The pairwise root mean square deviation was calculated among 30 refined structures for residues 18–104 and 126–146.

species were detected by autoradiography after exposure using direct exposure to films.

Fluorescence Anisotropy—The 23-bp oligonucleotide with a 3' reactive amine group (sequence 5'-CTC CAG GTC ACT GTG ACC TCC TC-3') was purchased from Sigma Genosys. It was covalently labeled with Alexa Fluor 488 succinimidyl ester dye (Invitrogen). A 10-fold molar excess of the dye was added to a solution of DNA in 0.1 M sodium borate, pH 9, buffer, and the reaction was allowed to proceed at room temperature for 3 h with continuous agitation. The reaction was stopped by adding 10% Tris-HCl 1 M. After ethanol precipitation, the labeled oligonucleotide was further purified using reversed-phase chromatography on a C₂-C₁₈ column. Finally, it was hybridized with a 1.1/1 molar excess of complementary strand. Steady-state fluorescence anisotropy binding titrations were carried out on a Tecan Sapphire II microplate reader, using a 470 nm light emitting diode for excitation, and a monochromator set at 530 nm (bandwidth 20 nm) for emission.

In Vitro Kinase Assays—*In vitro* phosphorylation of PknL and Rv2175c proteins was carried out for 30 min at 37 °C in a reaction mixture (20 μ l) containing buffer P (25 mM Tris-HCl, pH 7.0; 1 mM dithiothreitol; 5 mM MgCl₂; 1 mM EDTA) with 200 μ Ci/ml [γ -³²P]ATP. Phosphorylation of Rv2175c by PknL₁₋₂₈₁ was performed with 3 μ g of Rv2175c in 20 μ l of buffer P with 200 μ Ci/ml [γ -³²P]ATP and 500 ng of PknL₁₋₂₈₁ for 30 min at 37 °C. The reaction was stopped by addition of an equal volume of 2 \times sample buffer, and the mixture was heated at 100 °C for 5 min. After electrophoresis, gels were soaked in 16% trichloroacetic acid for 10 min at 90 °C, and dried. Radioactive proteins were visualized by autoradiography using direct exposure to films. *In vitro* phosphorylation for NMR, EMSAs, and mass

spectrometry analysis was performed as described above except that [γ - 32 P]ATP was replaced by 5 mM non-radioactive ATP and incubated overnight.

Mass Spectrometry Analysis—Purified Rv2175c was subjected to *in vitro* phosphorylation by PknL_{1–281} as described above with 5 mM cold ATP. Subsequent mass spectrometry analyses were performed as previously described (29).

RESULTS

Rv2175c Solution Structure—Rv2175c, a 146-amino acid protein with a calculated molecular mass of 16 kDa exhibits very weak similarity to transcriptional regulatory proteins harboring a DNA-binding domain (residues 32–52) with a helix-turn-helix (HTH) motif, as well as homologies to α -helix proteins like cyclins and cytochromes (17). Because bioinformatic analyses using several different web-based meta-servers failed to clearly identify Rv2175c as a typical DNA-binding protein, we decided to determine its structure, expecting that it would provide new insights with respect to its function. Rv2175c was isotopically labeled with 15 N, and 15 N- 13 C, expressed, and purified from *E. coli* carrying pET15bTev_Rv2175c. Following removal of its N-terminal His tag using TEV protease, purified Rv2175c was used for the structural determination by multidimensional NMR spectroscopy. By combining the information from the double and triple resonance heteronuclear experiments, we were able to assign all the amide group resonances (except Thr-29) for the non-proline residues (12 prolines), 93.8% of the other backbone resonances ($C\alpha$, C' , and $H\alpha$), 76.7% of the $C\beta$ resonances, and \sim 96% of the side-chain protons.

NMR experiments revealed that the N-terminal part (Met¹–Ile¹⁶) and a large loop (Thr¹¹⁰–Asn¹²²) of Rv2175c were fully disordered. The corresponding residues gave rise to the intense cross-peaks centered at 8.5 ppm in the HSQC spectrum (Fig. 1). Intriguingly, these two regions correspond to the less conserved parts of the protein found in different actinomycetes homologous proteins. Noteworthy, the loop Thr¹¹⁰–Asn¹²² is present in mycobacteria but missing constantly in *Corynebacterium* or *Streptomyces* despite a sequence identity close to 60% for the core residues (Fig. 2). In addition, multiple sequence alignments of Rv2175c homologues revealed that, except for *M. tuberculosis* and *Mycobacterium bovis*, most homologues, including *Mycobacterium smegmatis*, lack the first twelve residues (Fig. 2). One notable exception is *Mycobacterium avium paratuberculosis*, which carries a 20-amino acid extension with respect to the *M. smegmatis* sequence.

We solved the structure of Rv2175c, which corresponds to a monomer constituted of two domains with six α -helices and two β -strands in total (Fig. 3, A and B) with flexibility existing between the N-terminal (residues Pro¹⁸ to Val⁷⁷) and the C-terminal domains (residues Val⁷⁸ to Tyr¹⁴⁶). The 30 best structures were calculated and superimposed for the whole protein heavy atoms (except the first 16 residues) with a root mean square deviation of 1.1 Å, whereas the root mean square deviation calculated for the N-terminal or the C-terminal domain were of 0.7 Å and 0.85 Å, respectively (Fig. 4). Our data indicate that the N-terminal domain, with the topological α 1, α 2, β 1, and β 2 order, harbors an unusual prokaryotic winged helix-

turn-helix (wHTH) DNA-binding motif missing the typical third helix (30) (Fig. 3, A and B). To our knowledge, the only characterized HTH DNA-binding proteins missing the third helix are the bacteriophage protein from the Xis nucleoprotein filament (31). In the Rv2175c N-terminal domain, the turn following the second strand allows the next six residues (Ile⁶⁶ and Phe⁷¹) to cap the hydrophobic core formed by the two first helices of the wHTH, a role usually devoted to the third helix of the motif (Fig. 3C). Moreover, the Rv2175c C-terminal domain is composed of four anti-parallel helices (α 3– α 6) and their connecting turns together with a mobile 20-amino acid loop (residues Thr¹¹⁰–Asn¹²²). If most of the hydrophobic residues are buried in the helix bundle, some remain partially solvent-exposed (Leu⁸⁷, Val¹³⁸, and Tyr¹⁴⁶). Interestingly, in transcriptional regulators harboring a wHTH domain, the C-terminal segment usually possesses a dual role, a functional role as regulatory domain, and a structural role as an actor of protein dimerization when bound to DNA. The relative positioning of these two domains is dictated by contacts between the hydrophobic surface encompassing the residues from the C-terminal α -helices α 4 (Ile⁹⁸, Met⁹⁹, and Phe¹⁰³) and α 5 residues (Val¹²⁶ and Leu¹²⁹) and the N-terminal residues Val²² and Phe⁷⁰. Overall, the NMR solution structure determination of Rv2175c clearly identified structural features typically found in DNA-binding proteins with an original N-terminal wHTH domain as well as a C-terminal regulatory domain of unknown function.

Rv2175c Is a DNA-binding Protein—To confirm that Rv2175c is a DNA-binding protein two biochemical strategies were used. First, we confirmed by EMSA the ability of Rv2175c to bind non-relevant double-stranded DNA at low salt concentration. Because Rv2175c DNA targets remain unknown, the binding experiments were carried out using a typical assay mixture containing 50 mM NaCl with increasing amounts of purified Rv2175c. The results indicated that the Rv2175c protein interacted measurably with double-stranded DNA (Fig. 5A). An excess of cold DNA was also mixed along with the labeled probe, and the absence of a shifted probe indicated specificity of the binding activity of Rv2175c toward the probe.

DNA-binding activity of Rv2175c was further analyzed by fluorescence anisotropy determination, a method of choice to measure interaction between different molecules like protein/DNA. A 30-bp DNA segment was labeled with Alexa Fluor 488 dye and mixed with unlabeled Rv2175c. As expected, in the absence of salt, Rv2175c exhibited a substantial DNA-binding activity (Fig. 5C). However, increasing NaCl concentrations from 0 to 150 mM resulted in a dramatic decrease in the affinity for DNA, with a complete loss of activity culminating at 100 mM NaCl (Fig. 5C). The addition of salt raises the DNA-protein specificity and demonstrates that the anisotropy increase observed at low salt with the highest protein concentration is due to proper DNA-protein interactions, corresponding to a regain of specificity, rather than to a nonspecific aggregation. Taken together, our structural and biochemical data clearly establish the function of Rv2175c as a DNA-binding protein.

Rv2175c Is Phosphorylated on a Unique Threonine Residue—We recently showed that Rv2175c was exclusively phosphorylated on Thr residues, *in vitro* as well as *in vivo*, but the phosphorylation sites could not be identified (17). Therefore, to

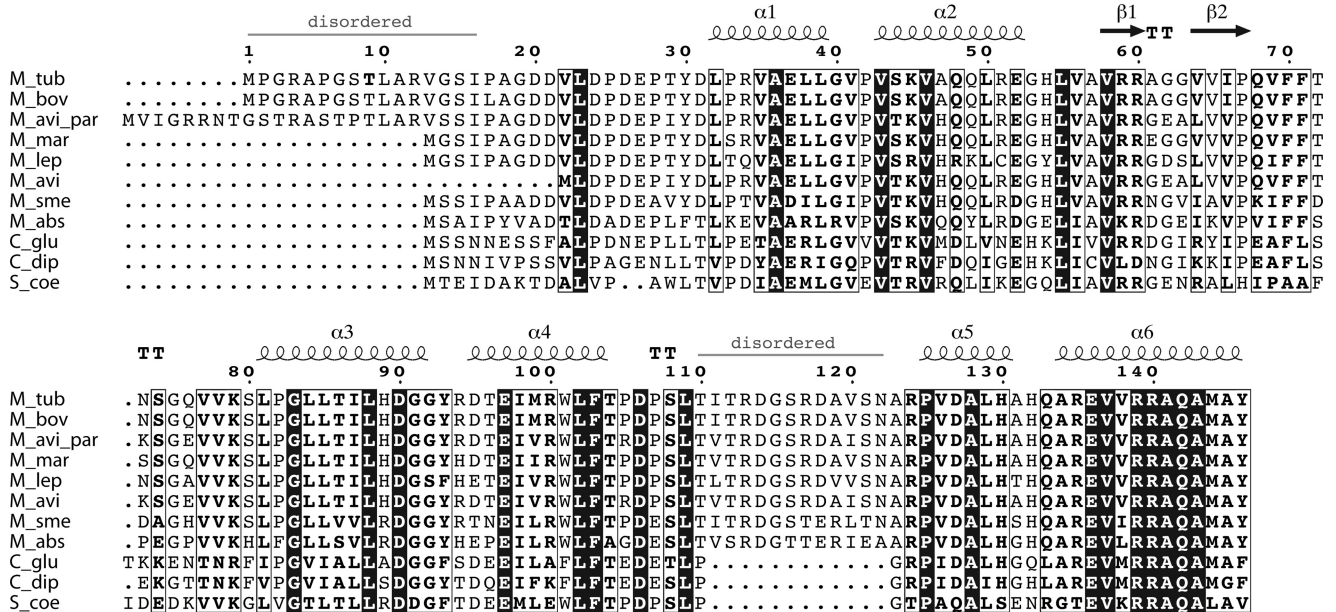


FIGURE 2. Multiple sequence alignment of Rv2175c ortholog proteins from corynebacteria and mycobacteria. Sequence alignment of the *M. tb* Rv2175c homologues in *M. bovis*, *M. avium paratuberculosis*, *M. marinum*, *M. leprae*, *M. avium*, *M. smegmatis*, *M. abscessus*, *Corynebacterium glutamicum*, *Corynebacterium diphtheriae*, and *Streptomyces coelicolor*. Protein secondary element assignments for Rv2175c are represented on the top of the sequences. Numbering of amino acids corresponds to the Rv2175c protein from *M. tuberculosis*.

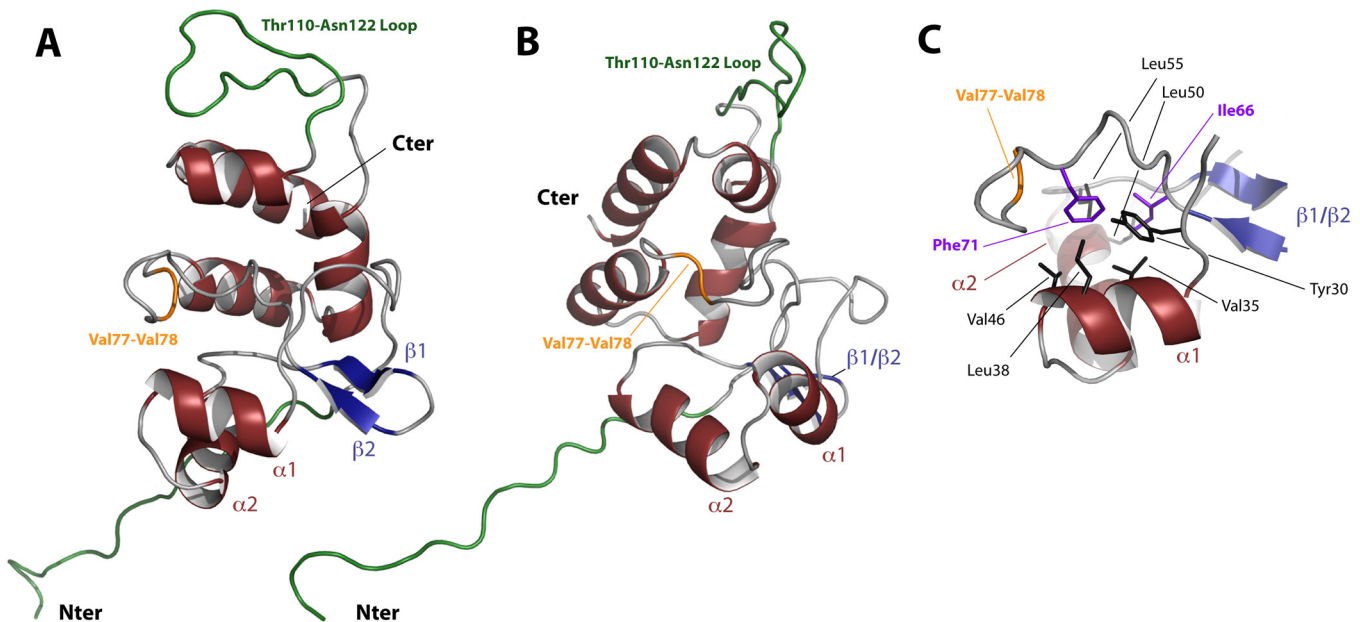


FIGURE 3. Overall structure of Rv2175c. A and B, two views related by a 90° rotation along the z axis of a schematic representation of the Rv2175c structure. The residues Met¹ to Ile¹⁶ and Thr¹¹⁰ to Asn¹²² are fully disordered and represented in green. C, close-up view of the internal face of the $\alpha 1$ and $\alpha 2$ helices. The N-terminal domain harbors an unusual prokaryotic wHTH DNA-binding motif missing the typical third helix. The turn after the second strand (Ile⁶⁶ and Phe⁷¹) caps the hydrophobic core formed by the two first helices of the wHTH, a role usually devoted to the third helix of the motif.

BL21(DE3)Star harboring pETPhos_Rv2175c_T9A, and used in an *in vitro* kinase assay. The recombinant Rv2175c_T9A was incubated along with [γ -³²P]ATP and PknL₁₋₂₈₁. The mixture was separated by SDS-PAGE and analyzed by autoradiography. As shown in Fig. 6B (upper panel), equal amounts of Rv2175c or mutant Rv2175c_T9A were used. Phosphorylation of Rv2175c_T9A was completely abrogated, compared with phosphorylation of Rv2175c, as evidenced by the absence of a specific radioactive band (Fig. 6B, lower panel). These results unambiguously demonstrate that Rv2175c_T9A has lost its

ability to be phosphorylated by PknL. An additional round of mass spectrometry analysis was also performed directly on Rv2175c_T9A pre-treated with ATP and PknL, which failed to identify any additional phosphate group that could eventually have arisen as a compensatory mechanism to the loss of the Thr⁹ phosphorylation (data not shown).

Phosphorylation on the Rv2175c N-terminal Extension Modulates Its DNA-binding Activity—The structural elucidation of Rv2175c as a DNA-binding protein and the identification of its phosphorylation site led to the hypothesis that phosphorylation

Solution Structure of *M. tuberculosis* Rv2175c

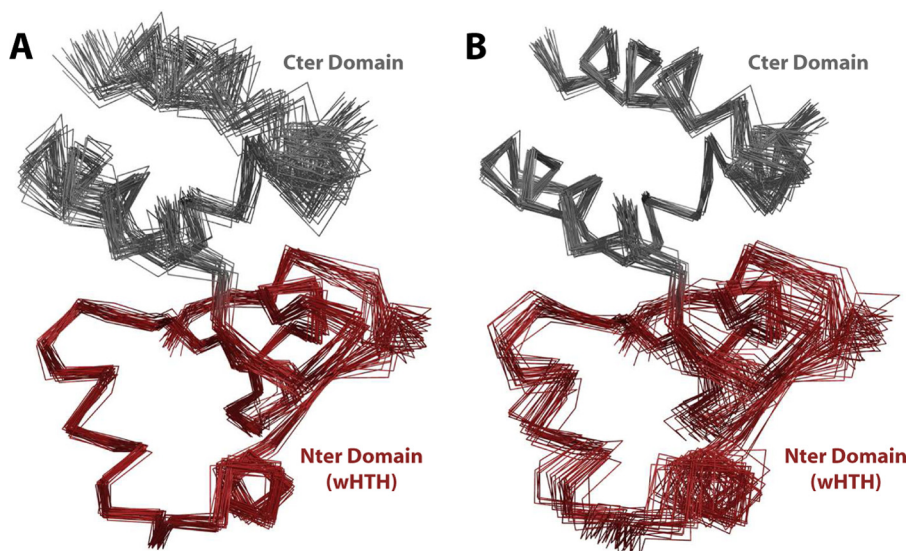


FIGURE 4. **Conformational flexibility in Rv2175c.** Representation of the final ensemble comprising 30 NMR structures of Rv2175c. The N-terminal wHTH domain is represented in red while the putative C-terminal effector domain is represented in gray. The residues Met¹ to Pro¹⁷ and Asp¹⁰⁶ to Ala¹²³ are not represented. The superimposition made on the sole wHTH domain (A) and the C-terminal domain (B) shows that some flexibility exists between the two domains.

may influence the DNA-binding activity of Rv2175c. Following a strategy that has been successfully used to demonstrate that regulation of a substrate protein via phosphorylation is important during active cell growth in mycobacteria (Wag31), or for mycolic acid metabolism (mtFabH) (9, 13), we expressed and purified the phosphorylation mimics Rv2175c_T9D or Rv2175c_T9E. Indeed, previous studies have shown that acidic residues such as Asp or Glu qualitatively recapitulate the effect of phosphorylation with regard to functional activity (32). The option was taken to analyze and compare the DNA-binding activity of Rv2175c, Rv2175c_T9D, or Rv2175c_T9E using non-relevant DNA by EMSA and by fluorescence anisotropy at various NaCl concentrations.

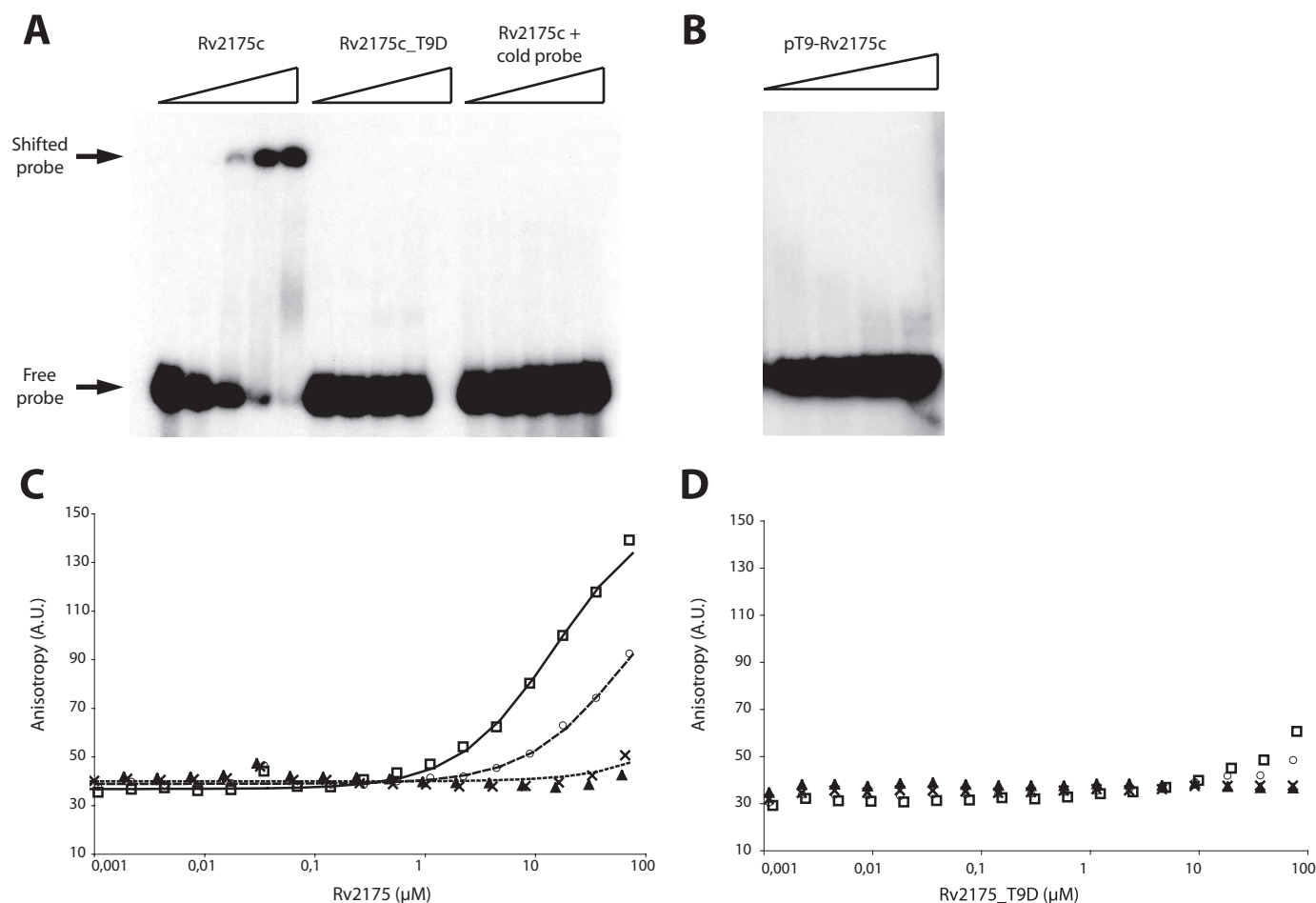


FIGURE 5. **DNA-binding activity of Rv2175c.** A and B, gel electrophoretic mobility shift assays of the binding of Rv2175c to a non-relevant 200-bp DNA fragment. The radioactive 200-bp DNA probe was incubated with 0.4, 0.6, 0.8, and 1 μ g of the purified Rv2175c, Rv2175c_T9D, or phosphorylated Rv2175c by PknL (pT9-Rv2175c) and analyzed by non-denaturing PAGE. As a control, non-radiolabeled DNA (cold probe) was added to the Rv2175c mix. C and D, anisotropy binding profile for binding of Rv2175c (B) and Rv2175c_T9D (C) to a 23-bp oligonucleotide labeled with Alexa Fluor 488 succinimidyl ester dye. The protein concentration was 4 nM. The buffer was 10 mM Tris-HCl, pH 7.5, with 0 mM NaCl (\square), 50 mM NaCl (\circ), 100 mM NaCl (\times), or 150 mM NaCl (\blacktriangle). The anisotropy measurements were performed four different times and showed consistent order of magnitude.

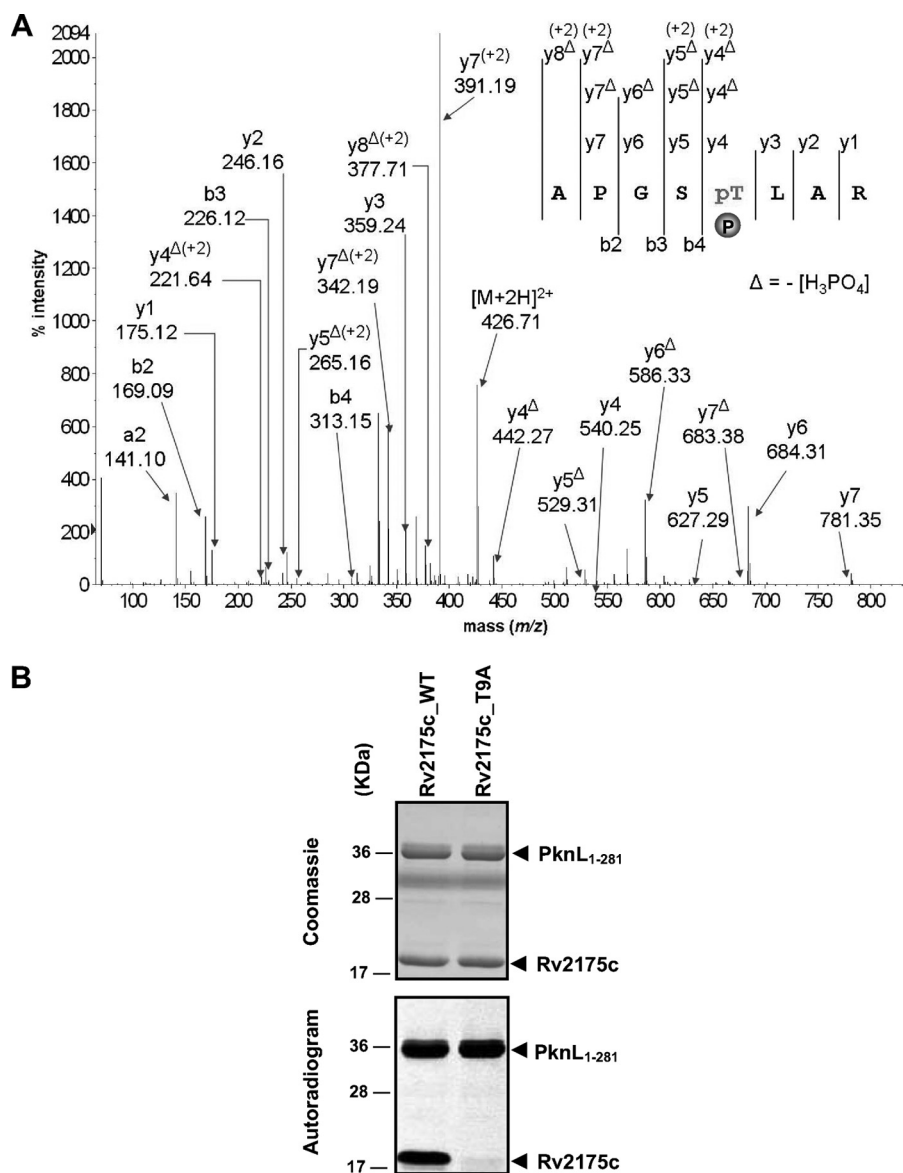


FIGURE 6. Identification of Rv2175c phosphorylation site. *A*, MS/MS spectrum of the doubly charged ion $[M+2H]^{2+}$ at m/z 426.7 of a peptide (5–12) (monoisotopic mass: 851.40 Da). Unambiguous location of the phosphate group on Thr⁹ was showed by observation of the “y” C-terminal daughter ion series. Starting from the C-terminal residue, all y ions lose phosphoric acid (–98 Da) after the Thr⁹-phosphorylated residue. *B*, *in vitro* phosphorylation of the Rv2175c_T9A mutant. Purified Rv2175c and Rv2175c_T9A were incubated with PknL_{1–281} and $[\gamma\text{-}^{32}\text{P}]\text{ATP}$. Samples were separated by SDS-PAGE (*upper panel*) and visualized by autoradiography (*lower panel*).

As mentioned above, the EMSAs were carried out using a radioactive 200-bp non-relevant DNA fragment, except that Rv2175c was substituted by Rv2175c_T9D or Rv2175c_T9E (data not shown). Although Rv2175c protein interacted with this double-stranded DNA, the Rv2175c_T9D and Rv2175c_T9E phosphorylation mimics failed to shift the probe, indicating that they had lost their ability to bind to DNA (Fig. 5A). On the contrary, EMSA carried out using a Rv2175c_T9A mutant, a mutation that prevents the phosphorylation of Rv2175c, showed that this mutant retained its DNA-binding activity (data not shown), thus confirming the critical role of phosphorylation in Rv2175c to inhibit the DNA binding. Moreover, EMSA assays were performed using Rv2175c phosphorylated by PknL in the presence of cold ATP, thus generating pT9-Rv2175c. As shown in Fig. 5B, the phospho-

rylated isoform of Rv2175c failed to bind DNA, thus confirming the critical role of phosphorylation to prevent DNA binding, as previously observed with the mimics mutants, T9D or T9E (Fig. 5A).

In addition, the fluorescence anisotropy method using the labeled 30-bp DNA fragment, which was mixed with unlabeled Rv2175c, Rv2175c_T9D, or Rv2175c_T9E, was performed to confirm the phosphorylation role in Rv2175c DNA-binding activity. As shown in Fig. 5C, Rv2175c exhibited a strong DNA-binding activity in the absence of salt, as expected whereas the affinity of Rv2175c_T9D for DNA in the absence of salt was comparable to that of the Rv2175c at 100 mM NaCl (Fig. 5D). Similar results were observed when Rv2175c_T9D was replaced by the other mimic mutant Rv2175c_T9E (data not shown). Together, these results indicate that mimicking phosphorylation by an acid residue at position 9 abrogates the DNA-binding activity of Rv2175c. This highlights the critical role of Thr⁹, which, following phosphorylation, negatively controls the DNA-binding activity of Rv2175c. This prompted us to investigate whether phosphorylation alters the structure of Rv2175c using two-dimensional and three-dimensional NMR experiments on the mimic mutants. However, our different analyses did not reveal major differences on a structural basis compared with the non-phosphorylated isoform of Rv2175c protein.

To investigate whether the N-terminal extension characterizing the *M. tb* protein was contributing to the DNA-binding activity of Rv2175c, fluorescence anisotropy of the Rv2175c mutant lacking the N-terminal extension (Rv2175c_{13–146}) was recorded using the same conditions as mentioned above. This truncated protein exhibited a DNA-binding activity comparable to the one of full-length protein (data not shown), indicating that the first 13 N-terminal residues are not involved in the DNA-binding activity of the protein in the absence of phosphorylation, but act as a phosphoacceptor site that regulates Rv2175c DNA-binding activity.

Effect of Thr⁹ Phosphorylation on Rv2175c Structural Organization—In a second set of experiments, PknL was purified and used to phosphorylate a ¹⁵N-labeled sample of Rv2175c. The first series of experiment was performed in the

Solution Structure of *M. tuberculosis* Rv2175c

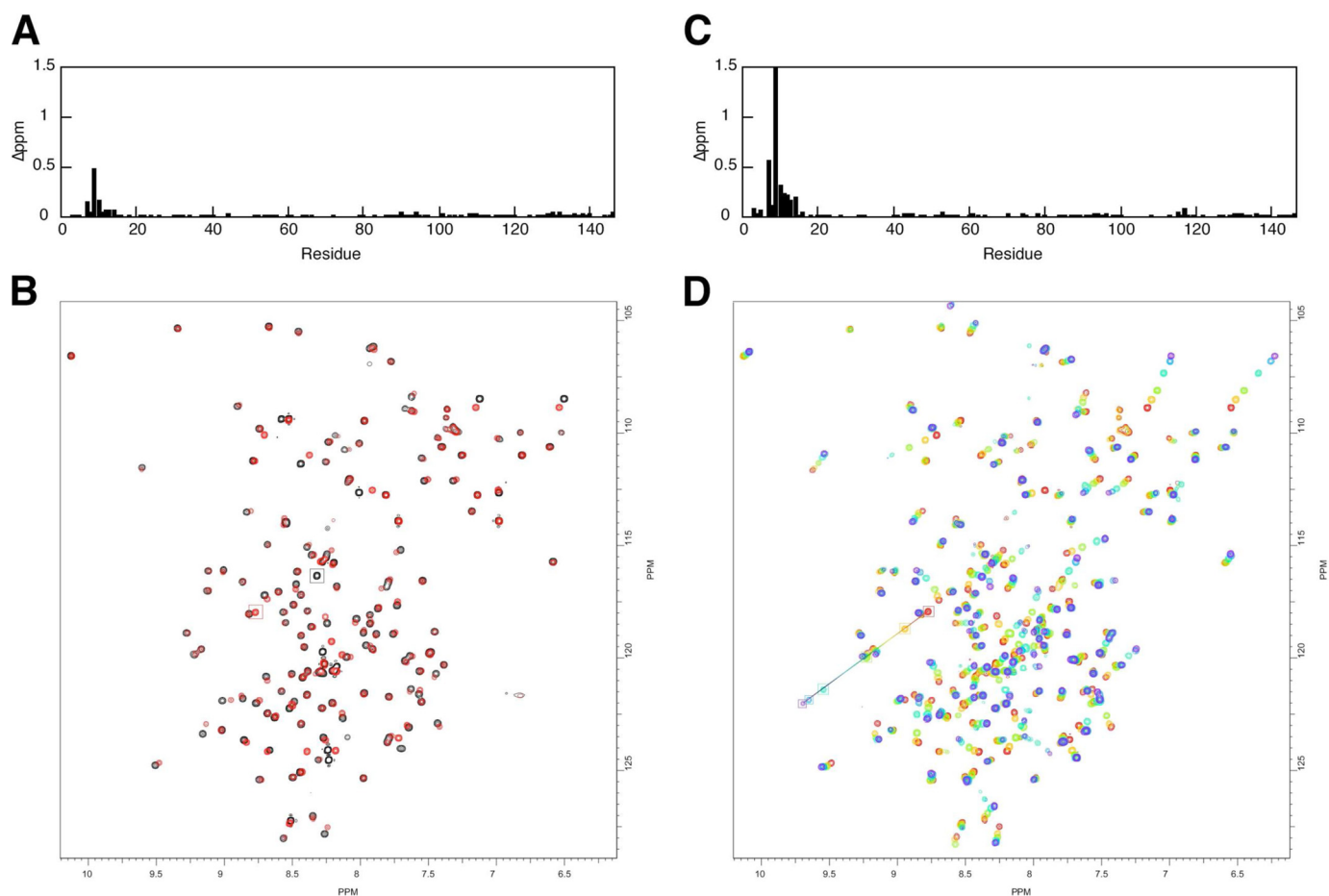


FIGURE 7. Chemical shift perturbations following Rv2175c phosphorylation. Amide averaged chemical shift differences ($\Delta\delta$) as a function of the protein sequence. $\Delta\delta$ values have been calculated between the amide group resonances of Rv2175c non-phosphorylated and Rv2175c phosphorylated by PknL (pRv2175c) using $\Delta\delta = [\Delta\delta_{\text{H}}^2 + (\Delta\delta_{\text{N}} \cdot \gamma_{\text{N}} / \gamma_{\text{H}})^2]^{0.5}$ at pH 4.6 (A) and pH 6.8 (C). The ¹H-¹⁵N HSQC spectrum shows superimposition of Rv2175c non-phosphorylated (in black) with pRv2175c (in red) at pH 4.6. The Thr⁹ and the phosphorylated Thr⁹ (pThr) resonances are squared in black and red, respectively (B). The ¹H-¹⁵N HSQC spectrum superimposition of pRv2175c at pH 4.6 (in red), pH 5.0 (in yellow), pH 5.3 (in light green), pH 6.1 (in dark green), pH 6.4 (in blue), and pH 6.8 (in purple). The pThr resonance is squared in the corresponding colors (D).

same conditions at pH 4.6, and a few chemical shift variations could be observed on the ¹H,¹⁵N HSQC spectrum recorded after treatment with the kinases (Fig. 7, A and B). Only the Thr⁹ residue and its close neighbors could be clearly detected, whereas no significant modifications of the Rv2175c core domain could be resolved by NMR for the phosphorylated isoform of Rv2175c in these conditions (Fig. 7B). Importantly, frequency resonance sequential attribution revealed a unique phosphorylation site on Thr⁹, clearly identified as the most important chemical shift change, thus confirming our mass spectrometry analysis (Fig. 6A), and that PknL was clearly able to phosphorylate Rv2175c despite an obvious structural shift that could explain the role of Thr⁹ phosphorylation. The down-field chemical shift change from Thr to pThr observed at pH 4.6 was around 0.5 ppm, compared to the 2 ppm observed in recent studies made at a higher pH (6.4) (21). Therefore, to determine whether the pH could be responsible for the failure to observe a structural shift, five samples of the protein were prepared at pH 4.6, 5, 5.3, 6.1, 6.4, or 6.8. However, due to instability as the pH increased, around 90% of the protein precipitated. Consequently, only limited NMR data were obtained, particularly the [¹H,¹⁵N] HSQC experiment using different acquisition time. Although we could not record any other experiment to solve

and compare the solution structures of the phosphorylated and non-phosphorylated isoforms at different pH, it is noteworthy that only the residue Thr (with a 1.5-ppm chemical shift) and its close neighbors were affected by phosphorylation without modifications of the core domain residues, indicating that pH did not affect any structural rearrangement (Fig. 7, C and D). It appears therefore tempting to hypothesize that PknL-dependent phosphorylation on Thr⁹ does not engender major structural modifications on the Rv2175c monomer. However, it remains possible that the inhibitory mechanism triggered by phosphorylation may disturb protein dimerization and/or induce a structural rearrangement between the N-terminal and the C-terminal domains, or an interaction with a third partner beside DNA.

DISCUSSION

Recent years have been characterized by a tremendous increase in structural information on protein-DNA complexes and uncovered a remarkable structural diversity in DNA binding folds (33). A subclass of the HTH family known as the wHTH proteins are so named due to the presence of an additional wing immediately C-terminal to the HTH unit that mediates additional contacts with the DNA (30). Here, we have

solved the solution structure of Rv2175c, which is characterized by the presence of an original N-terminal wHTH. This domain is associated with a putative regulatory C-terminal domain sharing no similarities with any structure solved to date. All structural features necessary for protein-DNA interactions are present, except the third helix of the wHTH tri-helical bundle domain, which is missing in Rv2175c, like in the bacteriophage protein from the Xis nucleoprotein filament (31), while the first two helices and the winged β -strand hairpin corresponding to the domains of the protein that directly interacts with the DNA are conserved.

Biochemical studies, including EMSA and fluorescence anisotropy, further confirmed that Rv2175c is capable to bind DNA at low salt concentrations. Taken, collectively, our data clearly establish the function of Rv2175c as a DNA-binding protein. Our biochemical studies uncovered that Thr⁹, laying within the N-terminal disordered extension, is the unique phosphoacceptor in Rv2175c. The presence of the phosphorylation site in a flexible region of the protein is likely to promote optimal presentation/interaction between the phosphorylation site and the kinase.

This work presents compelling evidence that Rv2175c encodes a DNA-binding protein and that this activity is inherent to the main core domain of the protein as a truncated version of Rv2175c protein lacking the first 13 residues presented the same DNA-binding properties than the wild-type Rv2175c. Importantly, Rv2175c mutants mimicking the phosphorylation isoform failed to express DNA-binding activity, supporting the view that phosphorylation of Thr⁹ negatively regulates Rv2175c activity. Surprisingly, structural comparison of the non-phosphorylated and PknL-phosphorylated isoforms of Rv2175c did not reveal major conformational changes. Our structural study revealed that Rv2175c behaves as a monomer in solution, a feature that may explain the failure to detect major structural changes. Because DNA-binding proteins, and particularly prokaryotic transcription factors, usually act as homodimers, one can speculate that phosphorylation of Thr⁹ interferes with cooperativity and/or oligomerization mechanisms linked to the DNA binding of a dimeric form of Rv2175c. Whether phosphorylation exerts its inhibitory effect on DNA binding by disrupting homotypic interactions between two monomers represents an attractive hypothesis. However, as a prerequisite to test this hypothesis, specific DNA target(s) of Rv2175c will have to be identified. Work is currently in progress to identify the putative regulon(s) controlled by Rv2175c using a chromatin immunoprecipitation (chip-on-chip) approach, which should lead to the Rv2175c-specific DNA targets and to determining their locations on a whole genome basis.

Multiple sequence alignments indicated that the disordered N-terminal sequence bearing the phosphoacceptor is only restricted to a few pathogenic mycobacterial species. In addition to *M. tb* and *M. bovis* a full conservation of this domain was found to be present in *M. africanum*, *M. microti*, and *M. canettii* (data not shown), but not in other pathogenic species such as *M. marinum* or *M. leprae* or in non-pathogenic species such as *M. smegmatis*. Overall, these observations support the occurrence of a regulation mechanism by phosphorylation of Rv2175c, which is unique to the *M. tuberculosis* complex. Dur-

ing the infection process, *M. tb* encounters numerous environmental conditions and induces or represses a number of genes for a quick adjustment to new conditions allowing the bacteria to adapt and survive within its host. Whether the phosphorylation-dependent mechanism controlling the activity of Rv2175c contributes to the adaptation of *M. tb* in its host requires further study.

Because these organisms display a complex life style comprising different environments and developmental stages, it is believed that their success results from their remarkable capacity to survive within the infected host, which is also linked to the presence of an unusual cell wall. It is therefore tempting to speculate that the PknL/Rv2175c couple participates in the modulation and adaptation of cell wall components in response to environmental changes. In this context it is important to mention that this kinase/substrate pair is present in the close vicinity of the *dcw* (division and cell wall synthesis) gene cluster, encompassing several genes involved in cell wall synthesis and cell division (17, 18). In addition, Kang *et al.* (34) demonstrated that the activity of Wag31, a homologue of the cell division protein DivIVA, is controlled by phosphorylation by mycobacterial STPKs and that Wag31 regulates cell shape and cell wall synthesis in *M. tb* in response to environmental signals mediated via STPK phosphorylation of Wag31. Depletion of Wag31 causes a dramatic morphological change in which one end of the cell becomes round rather than rod-shaped. Interestingly, *wag31* (Rv2145c) belongs to the 30-kb *dcw* cluster. Whether Rv2175c acts as a transcriptional regulator involved in controlling the *dcw* gene cluster has not been elucidated yet. Access to the DNA target(s) of Rv2175c may help to understand how regulation via phosphorylation of Rv2175c in response to environmental changes contributes to the persistence of *M. tb* within the infected host. A detailed characterization of the regulon(s) will be a major step in defining the role(s) of Rv2175c in the *M. tb* physiological adaptation to its environment.

In prokaryotes, protein kinases can be classified into two superfamilies based on their sequence similarities and enzymatic specifications: (i) the histidine kinase superfamily, which belongs to the two-component systems (1). In this system, the stimulus causes the histidine kinase to autophosphorylate a conserved histidine residue, forming a highly reactive phosphoramidate bond. The cognate response regulator catalyzes the phosphoryl transfer to a conserved aspartate within its own receiver domain. The phosphorylated response regulator interacts with transcription factors, which in turn, up- or down-regulate the number of genes; and (ii) the superfamily of serine, threonine, and tyrosine kinases (2, 3). *M. tb* has only twelve paired two-component systems homologues compared with more than 30 present in *E. coli* or *Bacillus subtilis*, which may be a consequence of the presence of a relatively much higher number of STPKs in *M. tb* (4). In addition to the proposed roles of STPKs in pathogenesis and development, it is likely that some STPKs simply fulfill the role of the classic bacterial two-component system regulatory proteins. In this context, the PknL/Rv2175c pair presents functional analogy with two-component systems, in that PknL can be compared with the sensor kinase, and Rv2175c as the transcriptional factor controlled by phosphorylation. In support of this view, PknH has been shown

Solution Structure of *M. tuberculosis* Rv2175c

to phosphorylates EmbR (encoded by its adjacent gene), a putative transcriptional regulator of arabinosyl transferases EmbCAB (35, 36). Activation of EmbR upon phosphorylation by PknH induces transcription from the *embCAB* operon, leading to a higher lipoarabinomannan/lipomannan ratio (37). Moreover, in a recent report, it was demonstrated that PknK (Rv3080c) phosphorylates the AraC/XylS transcriptional regulator VirS (Rv3082c), which regulates expression of the mycobacterial monooxygenase (*mymA*) operon, and that PknK-mediated phosphorylation of VirS increase its affinity for *mym* promoter DNA (38). These few examples highlight the functional analogy of *M. tb* STPKs in regulating the activity of DNA-binding proteins in a way similar to the classic two-component couples.

In conclusion, our study clearly established the function of Rv2175c as a DNA-binding protein, whose activity is controlled by phosphorylation of a unique residue in the N-terminal domain of the protein. However, future work is required to identify and characterize the DNA target(s) of Rv2175c and its possible link with the *dcw* gene cluster. In combination with structural analysis of the PknL/Rv2175c complex, these studies may also provide the key to designing molecules for selective disruption of signal transduction that are specific to *M. tb*.

Acknowledgments—We thank Dr. Emmanuel Margeat for help with fluorescence experiments, as well as Dr. Gilles Labesse and Jean-Luc Pons for helpful discussions. We also thank M. Becchi, I. Zanella-Cléon, and A. Cornut (Institut de Biologie et Chimie des Protéines, Lyon, France) for excellent expertise and technical assistance in mass spectrometry analysis.

REFERENCES

1. Stock, J. B., Ninfa, A. J., and Stock, A. M. (1989) *Microbiol. Rev.* **53**, 450–490
2. Hanks, S. K., Quinn, A. M., and Hunter, T. (1988) *Science* **241**, 42–52
3. Hunter, T. (1995) *Cell* **80**, 225–236
4. Cole, S. T., Brosch, R., Parkhill, J., Garnier, T., Churcher, C., Harris, D., Gordon, S. V., Eiglmeier, K., Gas, S., Barry, C. E., 3rd, Tekaia, F., Badcock, K., Basham, D., Brown, D., Chillingworth, T., Connor, R., Davies, R., Devlin, K., Feltwell, T., Gentles, S., Hamlin, N., Holroyd, S., Hornsby, T., Jagels, K., Krogh, A., McLean, J., Moule, S., Murphy, L., Oliver, K., Osborne, J., Quail, M. A., Rajandream, M. A., Rogers, J., Rutter, S., Seeger, K., Skelton, J., Squares, R., Squares, S., Sulston, J. E., Taylor, K., Whitehead, S., and Barrell, B. G. (1998) *Nature* **393**, 537–544
5. Av-Gay, Y., and Everett, M. (2000) *Trends Microbiol.* **8**, 238–244
6. Wehenkel, A., Bellinzoni, M., Graña, M., Duran, R., Villarino, A., Fernandez, P., Andre-Leroux, G., England, P., Takiff, H., Cerveñansky, C., Cole, S. T., and Alzari, P. M. (2008) *Biochim. Biophys. Acta* **1784**, 193–202
7. Sharma, K., Gupta, M., Krupa, A., Srinivasan, N., and Singh, Y. (2006) *FEBS J.* **273**, 2711–2721
8. Molle, V., Brown, A. K., Besra, G. S., Cozzzone, A. J., and Kremer, L. (2006) *J. Biol. Chem.* **281**, 30094–30103
9. Veyron-Churlet, R., Molle, V., Taylor, R. C., Brown, A. K., Besra, G. S., Zanella-Cléon, I., Fütterer, K., and Kremer, L. (2009) *J. Biol. Chem.* **284**, 6414–6424
10. O'Hare, H. M., Durán, R., Cerveñansky, C., Bellinzoni, M., Wehenkel, A. M., Pritsch, O., Obal, G., Baumgartner, J., Vialaret, J., Johnsson, K., and Alzari, P. M. (2008) *Mol. Microbiol.* **70**, 1408–1423
11. Villarino, A., Duran, R., Wehenkel, A., Fernandez, P., England, P., Brodin, P., Cole, S. T., Zimny-Arndt, U., Jungblut, P. R., Cerveñansky, C., and Alzari, P. M. (2005) *J. Mol. Biol.* **350**, 953–963
12. Dasgupta, A., Datta, P., Kundu, M., and Basu, J. (2006) *Microbiology* **152**, 493–504
13. Kang, C. M., Nyayapathy, S., Lee, J. Y., Suh, J. W., and Husson, R. N. (2008) *Microbiology* **154**, 725–735
14. Greenstein, A. E., MacGurn, J. A., Baer, C. E., Falick, A. M., Cox, J. S., and Alber, T. (2007) *PLoS Pathog.* **3**, e49
15. Park, S. T., Kang, C. M., and Husson, R. N. (2008) *Proc. Natl. Acad. Sci. U.S.A.* **105**, 13105–13110
16. Canova, M. J., Kremer, L., and Molle, V. (2009) *J. Bacteriol.* **191**, 2876–2883
17. Canova, M. J., Veyron-Churlet, R., Zanella-Cléon, I., Cohen-Gonsaud, M., Cozzzone, A. J., Becchi, M., Kremer, L., and Molle, V. (2008) *Proteomics* **8**, 521–533
18. Narayan, A., Sachdeva, P., Sharma, K., Saini, A. K., Tyagi, A. K., and Singh, Y. (2007) *Physiol. Genomics* **29**, 66–75
19. Cohen-Gonsaud, M., Barthe, P., Pommier, F., Harris, R., Driscoll, P. C., Keep, N. H., and Roumestand, C. (2004) *J. Biomol. NMR* **30**, 373–374
20. Canova, M. J., Kremer, L., and Molle, V. (2008) *Plasmid* **60**, 149–153
21. Barthe, P., Roumestand, C., Canova, M. J., Kremer, L., Hurard, C., Molle, V., and Cohen-Gonsaud, M. (2009) *Structure* **17**, 568–578
22. Sattler, M., Schleucher, J., and Griesinger, C. (1999) *Prog. NMR Spectrosc.* **34**, 93–158
23. Pons, J. L., Malliavin, T. E., and Delsuc, M. A. (1996) *J. Biomol. NMR* **8**, 445–452
24. Güntert, P. (2004) *Methods Mol. Biol.* **278**, 353–378
25. Cornilescu, G., Delaglio, F., and Bax, A. (1999) *J. Biomol. NMR* **13**, 289–302
26. Nederveen, A. J., Doreleijers, J. F., Vranken, W., Miller, Z., Spronk, C. A., Nabuurs, S. B., Güntert, P., Livny, M., Markley, J. L., Nilges, M., Ulrich, E. L., Kaptein, R., and Bonvin, A. M. (2005) *Proteins* **59**, 662–672
27. Laskowski, R. A., Moss, D. S., and Thornton, J. M. (1993) *J. Mol. Biol.* **231**, 1049–1067
28. Koradi, R., Billeter, M., and Wuthrich, K. (1996) *J. Mol. Graph.* **14**, 51–55, 29–32
29. Fiuza, M., Canova, M. J., Zanella-Cléon, I., Becchi, M., Cozzzone, A. J., Mateos, L. M., Kremer, L., Gil, J. A., and Molle, V. (2008) *J. Biol. Chem.* **283**, 18099–18112
30. Aravind, L., Anantharaman, V., Balaji, S., Babu, M. M., and Iyer, L. M. (2005) *FEMS Microbiol. Rev.* **29**, 231–262
31. Sam, M. D., Cascio, D., Johnson, R. C., and Clubb, R. T. (2004) *J. Mol. Biol.* **338**, 229–240
32. Cottin, V., Van Linden, A., and Riches, D. W. (1999) *J. Biol. Chem.* **274**, 32975–32987
33. Garvie, C. W., and Wolberger, C. (2001) *Mol. Cell* **8**, 937–946
34. Kang, C. M., Abbott, D. W., Park, S. T., Dascher, C. C., Cantley, L. C., and Husson, R. N. (2005) *Genes Dev.* **19**, 1692–1704
35. Molle, V., Kremer, L., Girard-Blanc, C., Besra, G. S., Cozzzone, A. J., and Prost, J. F. (2003) *Biochemistry* **42**, 15300–15309
36. Alderwick, L. J., Molle, V., Kremer, L., Cozzzone, A. J., Dafforn, T. R., Besra, G. S., and Fütterer, K. (2006) *Proc. Natl. Acad. Sci. U.S.A.* **103**, 2558–2563
37. Sharma, K., Gupta, M., Pathak, M., Gupta, N., Koul, A., Sarangi, S., Baweja, R., and Singh, Y. (2006) *J. Bacteriol.* **188**, 2936–2944
38. Kumar, P., Kumar, D., Parikh, A., Rananaware, D., Gupta, M., Singh, Y., and Nandicoori, V. K. (2009) *J. Biol. Chem.* **284**, 11090–11099